ADVANCES IN ATMOSPHERIC SCIENCES, VOL. 34, SEPTEMBER 2017, 1057–1068

• **Original Paper** •

Observation-based Estimation of Aerosol-induced Reduction of Planetary Boundary Layer Height

Jun ZOU[1,2], Jianning SUN*[1,2], Aijun DING[1,2], Minghuai WANG[1,2], Weidong GUO[1,2], and Congbin FU[1,2]

[1]*School of Atmospheric Sciences and Institute for Climate and Global Change, Nanjing University, Nanjing* 210023*, China*

[2]*Joint International Research Laboratory of Atmospheric and Earth System Sciences of Ministry of Education, Nanjing University, Nanjing* 210023*, China*

(Received 14 October 2016; revised 10 March 2017; accepted 26 April 2017)

ABSTRACT

Radiative aerosols are known to influence the surface energy budget and hence the evolution of the planetary boundary layer. In this study, we develop a method to estimate the aerosol-induced reduction in the planetary boundary layer height (PBLH) based on two years of ground-based measurements at a site, the Station for Observing Regional Processes of the Earth System (SORPES), at Nanjing University, China, and radiosonde data from the meteorological station of Nanjing. The observations show that increased aerosol loads lead to a mean decrease of 67.1 W m^{-2} for downward shortwave radiation (DSR) and a mean increase of 19.2 W m^{-2} for downward longwave radiation (DLR), as well as a mean decrease of 9.6 W m^{-2} for the surface sensible heat flux (SHF) in the daytime. The relative variations of DSR, DLR and SHF are shown as a function of the increment of column mass concentration of particulate matter ($PM_{2.5}$). High aerosol loading can significantly increase the atmospheric stability in the planetary boundary layer during both daytime and nighttime. Based on the statistical relationship between SHF and $PM_{2.5}$ column mass concentrations, the SHF under clean atmospheric conditions (same as the background days) is derived. In this case, the derived SHF, together with observed SHF, are then used to estimate changes in the PBLH related to aerosols. Our results suggest that the PBLH decreases more rapidly with increasing aerosol loading at high aerosol loading. When the daytime mean column mass concentration of $PM_{2.5}$ reaches 200 mg m^{-2}, the decrease in the PBLH at 1600 LST (local standard time) is about 450 m.

Key words: aerosol, radiation, atmospheric stability, surface sensible heat flux, planetary boundary layer height

Citation: Zou, J., J. N. Sun, A. J. Ding, M. H. Wang, W. D. Guo, and C. B. Fu, 2017: Observation-based estimation of aerosol-induced reduction of planetary boundary layer height. *Adv. Atmos. Sci.*, **34**(9), 1057–1068, doi: 10.1007/s00376-016-6259-8.

1. Introduction

Disregarding large-scale synoptic forcing, the growth of the planetary boundary layer (PBL) during daytime is mainly driven by surface heating and upper-PBL entrainment (Sühring et al., 2014). Since solar radiation provides the energy for surface sensible heat flux (SHF), the evolution of the PBL height (PBLH) is influenced directly by the diurnal variation of shortwave radiation. The entrainment process, which leads to the downward transfer of heat (as well as mass) into the PBL, also contributes to the growth of the PBLH. A well-accepted value of the ratio of entrainment heat flux to the surface heat flux during daytime is 0.2 (Stull, 1976). Therefore, the surface heat flux determines the daytime development of the PBL to a large extent. In a simplified mixed-layer model, the PBLH can be predicted when the surface heat flux and the profile of potential temperature are known (Stull, 1988; van Zanten et al., 1999; Fedorovich et al., 2004; Sun, 2009).

Aerosols play an important role in radiation transfer due to absorption and/or scattering in the atmosphere, and thus could have great influence on the evolution of the PBLH. By scattering and absorbing the solar radiation, aerosols reduce the downward shortwave radiation (DSR) reaching the Earth's surface (Chen et al., 1994). The shadowing effect of scattering aerosols reduces the SHF, and consequently decreases the PBLH (Barbaro et al., 2013). Ding et al. (2013a) reported an extreme air pollution event due to mixed biomass burning and urban plumes and found a substantial depression of the PBL due to a decrease in the solar radiation intensity reaching the ground by more than 70% together with a decrease in the surface SHF by more than 85% during the daytime. However, the heating effect of the absorbing aerosols on the PBLH is highly complicated, as it is related to the vertical distribution of aerosols (Yu et al., 2002; Johnson et al., 2008; Barbaro et al., 2013). Yu et al. (2002) showed that aerosol

* Corresponding author: Jianning SUN
Email: jnsun@nju.edu.cn

absorption decreases the surface heating and thus suppresses PBL development but, on the other hand, it increases the solar heating in the atmosphere and decreases the strength of capping inversion, leading to a rise in the PBLH that compensates its depression due to a reduction in the SHF. However, Barbaro et al. (2013) reported that aerosol-induced heating deepens the inversion layer and stabilizes the upper part of the PBL.

Many studies have been conducted to understand aerosols' radiative forcing (e.g., Bush and Valero, 2003; Satheesh and Moorthy, 2005; Yu et al., 2006; Liao et al., 2015) and the impact of aerosols on the vertical structure of the PBL (Kaufman et al., 2002; Yu et al., 2002; Gomes et al., 2008; Johnson et al., 2008; Mukund et al., 2014; Huang et al., 2016). The impacts of aerosols on SHF and the PBLH were discussed in some of these studies but were mainly based on numerical simulations. For instance, Wong et al. (2012) conducted a ten-day simulation of a wildfire event in California and reported a decrease in the PBLH of over 500 m associated with a reduction in the DSR by more than 250 W m^{-2}. Wang et al. (2015) simulated haze episodes in Northeast China in July 2008 and derived a decrease in the PBLH of about 33%. However, probably due to a lack of high quality simultaneous observations of aerosols and radiative flux data, direct evidence of the radiative effect of aerosol on the PBLH from observations is rare, and it therefore remains unclear to what extent current models can simulate the coupling between the PBLH and aerosols. In this study, we develop a method to quantitatively estimate aerosols' radiative effects on the PBLH, based on two years of continuous measurements of $PM_{2.5}$, solar radiation, and SHF at the Station for Observing Regional Processes of the Earth System (SORPES) supersite in Nanjing, China (Ding et al., 2013b).

2. Data and methods

2.1. *Observation site and measurements*

The $PM_{2.5}$ mass concentration, solar radiation, surface heat flux, and radiosonde data from 1 November 2011 to 31 February 2014 collected at the SORPES supersite (118°57′10″E, 32°7′14″N; altitude: 24 m) in the Xianlin campus of Nanjing University, in the suburbs of Nanjing (Ding et al., 2013a, 2013b) are used in this study. The $PM_{2.5}$ mass concentration is measured by a mass analyzer (SHARP-5030, Thermo Fisher Scientific, Massachusetts, USA), which is housed on the top floor of a laboratory building. The downward shortwave and longwave radiation fluxes are measured by a net radiometer (CNR4, Kipp & Zonen, Delft, The Netherlands), which is mounted in the observation yard at a height of 2.5 m above ground. The surface sensible and latent heat fluxes are measured by an eddy covariance system (CSAT 3A, Campbell Scientific, Utah, USA), which is also mounted in the observation yard, at a height of 2.2 m above the ground. The signals for the eddy covariance calculations are sampled at 10 Hz. Before calculating the turbulence statistics, the data are passed through a quality control procedure that involves the removal of incomplete data, dropouts, and spikes. Following Kaimal and Finnigan (1994), the coordinate system is transformed by aligning the x-axis along the mean wind velocity. Then, the kinematic heat flux ($\overline{w'\theta'}$) and the SHF ($c_p\rho\overline{w'\theta'}$, where c_p is the air specific heat capacity at constant pressure, and ρ is the air density) are computed at 30-min intervals, which is the widely-accepted duration for calculating turbulent fluxes (Nordbo et al., 2013). Corrections are applied for sonic virtual temperature (Schotanus et al., 1983). Radiosonde measurements are carried out at 0800 local standard time (LST) and 2000 LST at the meteorological station of Nanjing (118°46′48″E, 32°2′24″N), which is about 20 km to the southwest of the SORPES site.

2.2. *Data processing*

As the main goal of this study is to estimate the aerosol radiative effects on the PBLH, and the presence of clouds would introduce extra complexity in the data analysis and interpretation, we choose to analyze the data only under clear-sky conditions. As cloud observations are not carried out at the SORPES site, the clear-sky days are identified by visual inspection of the incoming solar radiation, following the method of Offerle et al. (2003). In this method, only those days on which the diurnal variation of the DSR shows a perfectly smooth curve are selected. To avoid possible misidentified cases of cloudy days, those days with maximum DSR of less than 300 W m^{-2} are excluded (as shown in Fig. 1, the DSR is still larger than 300 W m^{-2} on days with heavy air pollution, e.g., on 25 December, when the daytime $PM_{2.5}$ mass concentration exceeds 200 μg m^{-3}, suggesting that the extreme low DSR value is caused by cloud). With these criteria, 270 days are selected for further analysis.

To investigate how air pollution reduces solar radiation and hence the PBLH, we identify the "clean" days among the 270 selected days as a reference in each month. As the $PM_{2.5}$ concentration is generally high in Nanjing, the reference days are chosen as the days upon which the largest maximum daytime DSR among those days with a daytime 30-min mean $PM_{2.5}$ concentration is less than 40 μg m^{-3} (the observational data show that several days exist in each month whose daytime 30-min mean $PM_{2.5}$ concentration is less than

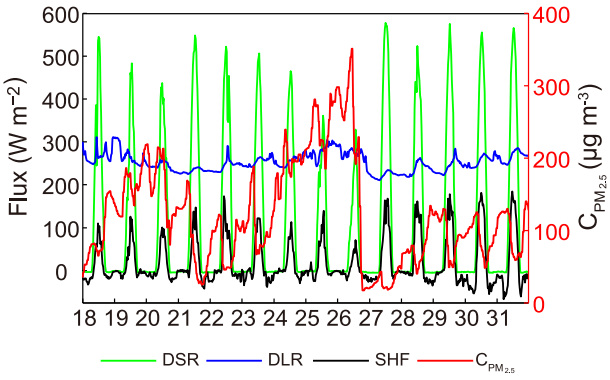

Fig. 1. Time series of DSR, DLR, SHF, and $PM_{2.5}$ mass concentration during 18–31 December 2013.

40 μg m^{-3}, and the statistics are given in Table 1).

2.3. *Prediction of the daytime PBLH*

During daytime, the development of the convective boundary layer (CBL) is driven by the surface heating, if we disregard the influence of background wind (Stull, 1988). The growth rate of the PBLH can then be characterized by a simplified parameterization (Sun, 2009), in which only the surface heat flux and the background stratification are needed. This parameterization is expressed as

$$\frac{\mathrm{d}z_i}{\mathrm{d}t} = \frac{1+A_\mathrm{e}}{\beta}\frac{\overline{w'\theta'_s}}{\gamma z_i}\,, \tag{1}$$

where z_i is the boundary layer height; A_e is the entrainment flux ratio, which is defined as the ratio of the downward heat flux at the CBL top to the upward heat flux at the surface, and is approximately a constant of 0.2 (Stull, 1976; Deardorff et al., 1980; Fedorovich et al., 2004; Sun, 2009); $\overline{w'\theta'_s}$ is the surface kinematic heat flux; γ is the lapse rate of the potential temperature in the free atmosphere above the CBL; and β is a parameter characterizing the relative stratification of the entrainment zone at the CBL top, which is approximately a constant of 0.9 for a purely buoyancy-driven CBL (Deardorff et al., 1980; Fedorovich et al., 2004; Sun, 2009).

Rewriting Eq. (1) gives the prediction formula of the PBLH as follows:

$$z_{i_2}^2 - z_{i_1}^2 = \frac{2(1+A_\mathrm{e})}{\beta\gamma}\frac{Q_H}{c_p\rho}(t_2 - t_1)\,, \tag{2}$$

where Q_H is the SHF, and equals $c_p\rho\overline{w'\theta'_s}$. Q_H can be calculated synchronously from the $\overline{w'\theta'_s}$ via the eddy covariance system, since the air pressure is measured and ρ can be obtained. Equation (2) is then used to predict the PBLH. The time step $\Delta t = (t_2 - t_1)$ is 30 min. The lapse rate of potential temperature γ is obtained from the radiosonde data obtained at Nanjing Observatory at 0800 LST, which is the initial time for the prediction. The PBLH at 0800 LST can also be derived from the radiosonde data. It is defined as the height at which the vertical gradient of potential temperature has a maximum value (Stull, 1988; Batchvarova and Gryning, 1991). According to the mean values of the PBLH derived from the radiosonde data in different seasons, the initial values of the PBLH are set as follows: 50 m in winter; 100 m in spring and autumn; and 200 m in summer. We assume that the profile of the potential temperature above the CBL remains unchanged during the daytime, which allows the predicting model of the PBLH to perform satisfactorily under steady synoptic conditions (Batchvarova and Gryning, 1991). These assumptions are not expected to significantly influence our results, as we mainly focus on the change in the PBLH caused by the decrease in the SHF associated with air pollution loads.

2.4. *Calculation of the aerosol impact on DSR, DLR and SHF*

We first estimate the column aerosol burden in the PBL. As we do not have the observations of the vertical profile of $PM_{2.5}$, a uniform distribution of $PM_{2.5}$ is assumed in the PBL during the daytime, which is a reasonable assumption given that the PBL is generally well-mixed (Liu et al., 2009). The column concentration is then approximated as:

$$\mathrm{CC}_{\mathrm{PM}_{2.5}} = C_{\mathrm{PM}_{2.5}} z_i\,, \tag{3}$$

Table 1. The mean values of DSR, DLR, SHF and $PM_{2.5}$ mass concentration during the daytime. The annual mean is the average from the seasonal means rather than from the daily means (Ding et al., 2008), the differences in brackets are the percentages of difference over the mean background values.

	DSR (W m^{-2})	DLR (W m^{-2})	SHF (W m^{-2})	$PM_{2.5}$ (μg m^{-3})
Annual mean (number of days: 270)				
Average	366.5	339.4	75.0	72.7
Background	433.6	320.2	84.6	34.3
Difference	−67.1 (−15.5%)	19.2 (6.0%)	−9.6 (−11.3%)	38.4 (112.0%)
Spring mean (number of days: 49)				
Average	446.3	330.3	109.7	66.9
Background	498.5	310.0	120.3	38.0
Difference	−52.2 (−10.5%)	20.3 (6.5%)	−10.6 (−8.8%)	28.9 (76.1%)
Summer mean (number of days: 34)				
Average	432.6	436.6	57.1	42.3
Background	514.7	429.9	61.2	30.2
Difference	−82.1 (−16.0%)	6.7 (1.6%)	−4.1 (−6.7%)	12.1 (40.1%)
Autumn mean (number of days: 86)				
Average	326.5	326.3	68.7	77.7
Background	398.0	305.9	85.6	32.8
Difference	−71.5 (−18.0%)	20.4 (6.7%)	−16.9 (−19.7%)	44.9 (136.9%)
Winter mean (number of days: 101)				
Average	260.6	264.4	64.4	103.9
Background	323.3	234.8	71.2	36.1
Difference	−62.7 (−19.4%)	29.6 (12.6%)	−6.8 (−9.6%)	67.8 (187.8%)

where $C_{PM_{2.5}}$ is the mass concentration of $PM_{2.5}$ measured at surface, z_i is the PBLH predicted by the method described in section 2.3. Aerosol optical depth (AOD) would be another parameter directly linked to the column aerosol burden. We compared the calculated $CC_{PM_{2.5}}$ values to the AOD data observed using a sunphotometer (CE-318, Cimel Electronique, Paris, France) located at the Gulou campus of Nanjing University, in the downtown area of Nanjing (Zhuang et al., 2017). The results show that they agree well with each other (see Appendix A). Then, any increase in the column concentrations compared to that on the reference days is calculated as

$$\Delta CC_{PM_{2.5}} = CC_{PM_{2.5}} - CC_{PM_{2.5,b}} , \quad (4)$$

where $CC_{PM_{2.5,b}}$ (the subscript "b" denotes "background") is the mean column concentration on the reference days (see the definition in section 2.2). Since DSR, DLR and SHF have strong seasonal and diurnal variations, the absolute changes in these variables may be dominated by their seasonal and diurnal variations and may not represent the true impact of aerosols. The relative changes of these variables are therefore used in the analysis and are defined as:

$$\frac{\Delta R_S}{R_{S_b}} = \frac{(R_S - R_{S_b})}{R_{S_b}} , \quad (5)$$

$$\frac{\Delta R_L}{R_{L_b}} = \frac{(R_L - R_{L_b})}{R_{L_b}} , \quad (6)$$

$$\frac{\Delta Q_H}{Q_{H_b}} = \frac{(Q_H - Q_{H_b})}{Q_{H_b}} . \quad (7)$$

Here, R_S, R_L and Q_H are the mean DSR, DLR and SHF, while R_{S_b}, R_{L_b} and Q_{H_b} are the values on the reference days, respectively. The relationships between $\Delta R_S/R_{S_b}$ and $\Delta CC_{PM_{2.5}}$, between $\Delta R_L/R_{L_b}$ and $\Delta CC_{PM_{2.5}}$, and between $\Delta Q_H/Q_{H_b}$ and $\Delta CC_{PM_{2.5}}$, are then analyzed for the time period of 1000 to 1600 LST of a day. The selection of the measuring time period takes account of the following important factors for this period: (i) the CBL is well developed, under which condition the distribution of aerosols could be considered as vertically uniform; (ii) the solar zenith angle is relatively small, so that the column mass concentration of $PM_{2.5}$ can therefore well represent the amount of aerosols in the light path; (iii) the magnitude of the SHF is relatively large, and relatively small measurement errors of about 10%–20% are expected (Kessomkiat et al., 2013).

3. Results

3.1. *Overall statistics*

The mean values of DSR, DLR, SHF and $PM_{2.5}$ mass concentration during the daytime for the whole period and for each season are calculated and compared with those on the clean days, and the statistics are listed in Table 1. Considering the seasonal change of the daytime duration, daytime is defined as 0700–1800 LST in spring (March–May) and autumn (September–November), 0600–1900 LST in summer (June–August), and 0800–1700 LST in winter (December–February), respectively.

The results in Table 1 show that the background mean magnitude of the $PM_{2.5}$ mass concentration during the daytime for different seasons falls within the range of 30–40 $\mu g\ m^{-3}$, implying that the background aerosol loading in Nanjing is relatively high, as compared to the clean areas. The highest mass concentration of $PM_{2.5}$ occurs in winter, in which the daytime mean magnitude exceeds 100 $\mu g\ m^{-3}$. In spring and autumn, the $PM_{2.5}$ mass concentration is still relatively high, and the daytime mean magnitude is 66.9 $\mu g\ m^{-3}$ and 77.7 $\mu g\ m^{-3}$, respectively. Summer has the lowest $PM_{2.5}$ mass concentration, whose daytime mean magnitude is smaller than 50 $\mu g\ m^{-3}$. The causes of the seasonal pattern have already been discussed by Ding et al. (2013b). The main reasons include long-range transport influenced by the Asian monsoon, different vertical mixing due to different PBLHs, and seasonal emission differences.

Table 1 shows that summer has the largest daytime decrease in DSR (82.1 W m^{-2}), while the surface $PM_{2.5}$ concentration reaches its minimum. One reason is that solar radiation is strongest in summer and the same aerosol loading might result in a relatively large decrease in the absolute value of DSR in this season. Another reason is that the PBLH is highest in summer due to solar insolation, resulting in a comparable column concentration with other seasons, even though the ground $PM_{2.5}$ concentration is low. This is why we consider using the aerosol column concentration to explore the relationship between aerosols and solar radiation or SHF (see section 2.4).

It is known that a decrease in incoming solar radiation reduces the SHF. However, it is interesting that the largest aerosol-induced decrease in DSR is associated with the smallest reduction in SHF in summer. This may be due to the relatively high soil humidity in this season, because in the eastern China summer, especially in June–July, it is the rainy season. Thus, the SHF is usually smaller than the surface latent heat flux, and is less sensitive to a decrease in incoming solar radiation. In autumn, it is the dry season in this region; the decrease in DSR is slightly smaller than in summer, but the decrease in SHF is largest. Nevertheless, the measurement data show that the higher aerosol loading corresponds to a larger decrease in SHF, and an approximately linear relationship between the column mass concentration of $PM_{2.5}$ and the decrease in SHF can be found (as will be shown later).

The DLR data given in Table 1 also indicate the role of the PBL absorbing aerosols in heating the atmosphere and hence enhancing the emissions of longwave radiation. On the other hand, the increase in DLR is largest in winter, when there are more absorbing aerosols in the PBL. As mentioned before, the heating effect of the absorbing aerosols on the atmosphere can change the atmospheric stability and influence the development of the PBL (Yu et al., 2002; Johnson et al., 2008; Barbaro et al., 2013; Ding et al., 2013b). Since we have no observations of the vertical distribution of absorbing aerosols, only the influence of aerosol scattering and absorption on the SHF and PBLH is discussed in this study.

To further understand the aerosol radiative effects on the solar radiation, SHF and PBLH, a heavy air pollution episode, which occurred in December 2013, is selected to show the continuous variation of the relevant variables. The time series of the DSR, DLR, SHF and $PM_{2.5}$ mass concentration during 18–31 December 2013 are plotted in Fig. 1. From 18 to 20 December, the $PM_{2.5}$ mass concentration increases from lower than 50 μg m^{-3} to over 200 μg m^{-3}, while the daily DSR peaks decrease gradually together with a weak increase in the DLR. The SHF shows no obvious varying trend. However, from 21 to 26 December, the $PM_{2.5}$ mass concentration increases from lower than 50 μg m^{-3} to above 300 μg m^{-3}, and the peak value of DSR decreases from about 550 W m^{-2} to only 330 W m^{-2}. At the same time, the DLR increases together with an obvious decrease in the SHF. These results indicate that the DSR is directly related to the aerosol loading, while the effect of aerosols on the SHF likely needs an accumulating process in a relatively long period.

The variation of the DLR is inevitably influenced by several factors: on the one hand, the increase in aerosols may also contribute to the increase in the DLR, because the absorption aerosols, such as black carbon (BC), could heat the atmosphere and thus cause an increase in the DLR at the surface; while on the other hand, other factors, such as atmospheric temperature, could also influence the DLR. The continuous increase in the DLR on 26 December could be due to the increase in atmospheric temperature at ground level (see Fig. 1). This case provides clear observational evidence for how atmospheric aerosols can influence surface fluxes. Statistics based on the selected 270 days during the two years could provide a more quantitative understanding of their relationship.

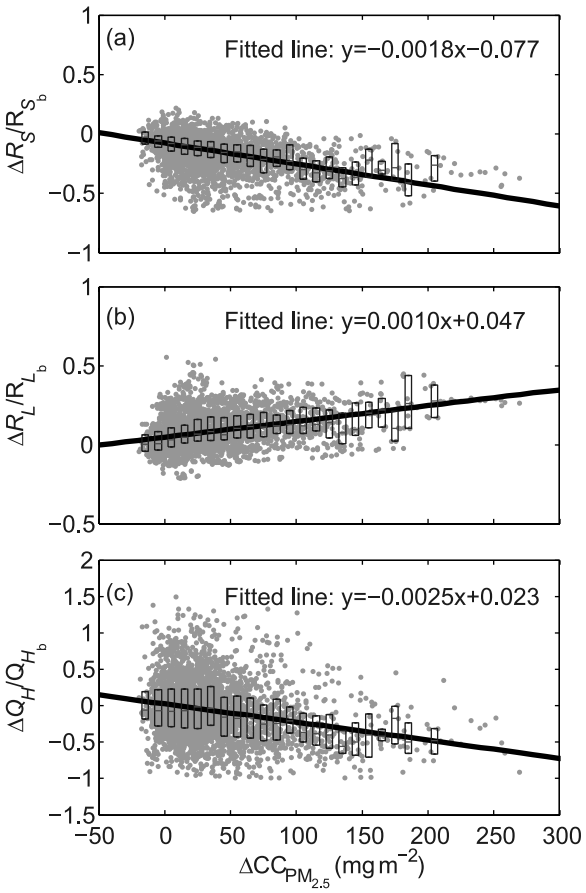

Fig. 2. The median (short lines) and inter-quartile range (boxes) of the relative change in (a) DSR, (b) DLR and (c) SHF, as a function of the increment of the column mass concentration of $PM_{2.5}$. The solid lines represent the linear fit of the data, and the fitting formulas are also given.

3.2. *Impacts of aerosols on radiation fluxes and the SHF*

The two-year statistics show clear evidence of aerosol influences on radiative fluxes and surface SHFs. The annual-mean DSR is about 16% less than that on the reference days, while the annual-mean SHF is about 11% less than that on the reference days. Data from different seasons show similar aerosol influences on radiative fluxes and SHFs. For example, Fig. 2 shows scatterplots of the relative changes in DSR, DLR and SHF versus changes in column aerosol concentrations. The relative change in DSR, DLR and SHF increases (in their absolute values) with the increase in the column mass concentration of $PM_{2.5}$. With $\Delta CC_{PM_{2.5}}$ at about 300 mg m^{-2}, which is equivalent to a $PM_{2.5}$ concentration of about 300 μg m^{-3}, the decrease in the DSR could be higher than 50% and the increase in the DLR could be as high as 35%, while the change in the SHF could reach 70%. As SHF is also affected by many other factors, the data points in Fig. 2c are relatively scattered compared with those for the DSR and DLR. However, statistical testing suggests that the correlation between SHF and $\Delta CC_{PM_{2.5}}$ becomes significant. It should be noted here that, to simplify the problem, we assume the relative change in SHF as a linear function of the increase in the column mass concentration of $PM_{2.5}$, because the processes involved in the response of SHF change to the increase in aerosol loading are complex, but we have no evidence to describe the relationship between them using other functions in this study.

Our measurements indicate that the absolute values of relative change in DSR, DLR and SHF increase during the daytime, especially in the afternoon, on the air pollution days (not shown), suggesting the accumulation of aerosols in the PBL. Figure 3 gives the statistics of the correlation between the measured $PM_{2.5}$ mass concentration and the estimated $PM_{2.5}$ column mass concentration. It can be seen that when the $PM_{2.5}$ mass concentration is relatively high (for example: higher than 100 μg m^{-3}) the $PM_{2.5}$ column mass concentration increases during the daytime. Because the real SHF on the polluted days is used to predict the PBLH, which should be smaller than that on the clean days, it is expected that the $PM_{2.5}$ column mass concentration is properly estimated. The increase in the $PM_{2.5}$ column mass concentration is caused by the accumulation of aerosols in the atmospheric column. On the other hand, the PBLH is estimated by using the potential temperature profile at 0800 LST, which is assumed to be unchanged during the daytime under well-mixed conditions. However, this treatment may induce some uncertainties in the

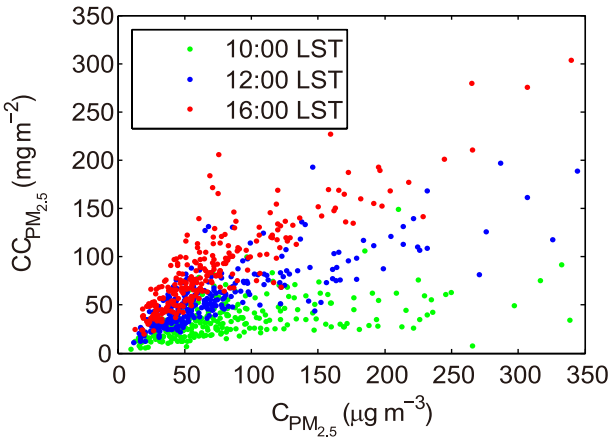

Fig. 3. Comparison between the measured $PM_{2.5}$ mass concentration at the surface and the estimated $PM_{2.5}$ column mass concentration in the atmospheric boundary layer at 1000 LST, 1200 LST and 1600 LST, respectively.

estimated PBLH on the polluted days. The effects of aerosols on the vertical distribution of the potential temperature will be discussed in the next section.

3.3. *Impacts of aerosols on PBL stratification*

The aerosols' radiative forcing can lead not only to cooling at the surface but also to heating of the PBL. The heating effect of absorbing aerosols (e.g., BC) changes the stability in the atmospheric boundary layer (Kaufman et al., 2002, Yu et al., 2002, Gomes et al., 2008, Johnson et al., 2008, Mukund et al., 2014, Huang et al., 2016). The numerical simulation results in Huang et al. (2016) show that the heating effect of BC stabilizes the atmosphere in the PBL. To elucidate the impacts of aerosols on PBL stratification, the profiles of mean potential temperature (Θ) and its gradient ($\partial\Theta/\partial z$) between low polluted days (mean daytime or nighttime $PM_{2.5}$ mass concentration lower than 75 μg m^{-3}) and high polluted days (mean daytime or nighttime $PM_{2.5}$ mass concentration higher than 75 μg m^{-3}) are compared at 0800 LST and 2000 LST, respectively.

Figure 4a shows the mean potential temperature profiles at 0800 LST for both low and high polluted days (to make a clearer comparison, the potential temperature minus the surface value is drawn). The cooling effect of longwave emissions from the surface during the nighttime produces a stably stratified atmosphere above the ground. This process continues till sunrise. It can be seen that the stratification in the near-surface layer is more stable on the high polluted days than on the low polluted days, which means that the growth rate of the PBLH is suppressed during the morning of high polluted days because, after sunrise, the CBL will develop in a more stably stratified background atmosphere. Figure 4b shows the mean profiles of potential temperature gradient at 0800 LST on these two kinds of air pollution days. In the layer over the surface, the vertical gradient of the potential temperature on the high polluted days is significantly larger than that on the low polluted days. This layer is relatively shallow and its depth is about 400–500 m in spring and autumn. However, this layer is relatively thick and its depth can extend to about 1000 m in summer and winter. As shown in Fig. 4b, in winter time, the atmosphere above 1000 m is less stable on the high polluted days than on the low polluted days. Therefore, if the CBL can exceed 1000 m, its growth rate will be greater on heavy polluted days than on low polluted days, which can compensate the depression of the PBLH due to the reduction in SHF, as discussed in Yu et al. (2002). However, it is difficult for this situation to occur because the radiosonde data suggest that the mean residual layer height at 2000 LST in winter is about 1000 m (the residual layer height can be regarded as the maximum PBLH during the daytime). It is interesting that this layer in summer is deeper than in spring and autumn. The reason is not clear and should be investigated further.

Figure 5 compares the profiles of mean potential temperature and its gradient at 2000 LST between the low and high polluted days. As 2000 LST is after sunset, the near-surface inversion layer has been established in each season (Fig. 5a), in which the vertical gradient of the potential temperature is larger than zero (Fig. 5b). Above this layer is the layer with constant potential temperature on the low polluted days (Fig. 5a), which corresponds to the mixed layer during daytime. This is the so-called residual layer, in which the vertical gradient of the potential temperature is approximately zero (Fig. 5b). However, on the high polluted days in autumn and winter, there is no strict residual layer right after sunset, because the potential temperature is not height-constant (Fig. 5a) and the vertical gradient of the potential temperature is obviously larger than zero, especially in winter (Fig. 5b). This means that, during the daytime, the heating of the ground surface is less pronounced due to the absorption of solar irradiance by the high aerosol load. Numerical simulations show that the shortwave heating rate induced by the unit mass of absorbing aerosols (i.e., BC) increases with height in the PBL due to the same vertical distribution of the solar irradiance (Ding et al., 2016). Thus, a stabilized CBL and a reduction in the upward velocity of the rising thermals is observed. According to the thermal theory of the CBL (Stull, 1988), this effect will weaken the entrainment process and hamper CBL development. Therefore, in addition to a decrease in the SHF, the CBL growth rate may be suppressed by the heating effect of the absorbing aerosols during the daytime. In the present study, this effect is not considered, and the predicted PBLH on high polluted days may be somewhat overestimated. As shown in Fig. 5, the suppression of the PBLH by aerosols is not found in spring. Observations in China suggest that, in this season, the absorbing aerosol loading is relatively low (Feng et al., 2014; Zhao et al., 2015).

3.4. *Estimation of aerosol-induced reduction of the PBLH*

To reveal the influence of aerosols on the PBLH, the corresponding SHF under the condition of no increment of $PM_{2.5}$ loading should be known. Thus, the SHF on the clean days (i.e., $Q_{H_{\rm cln}}$, where the subscript "cln" denotes "clean day") should be retrieved from the real SHF data. Then, the

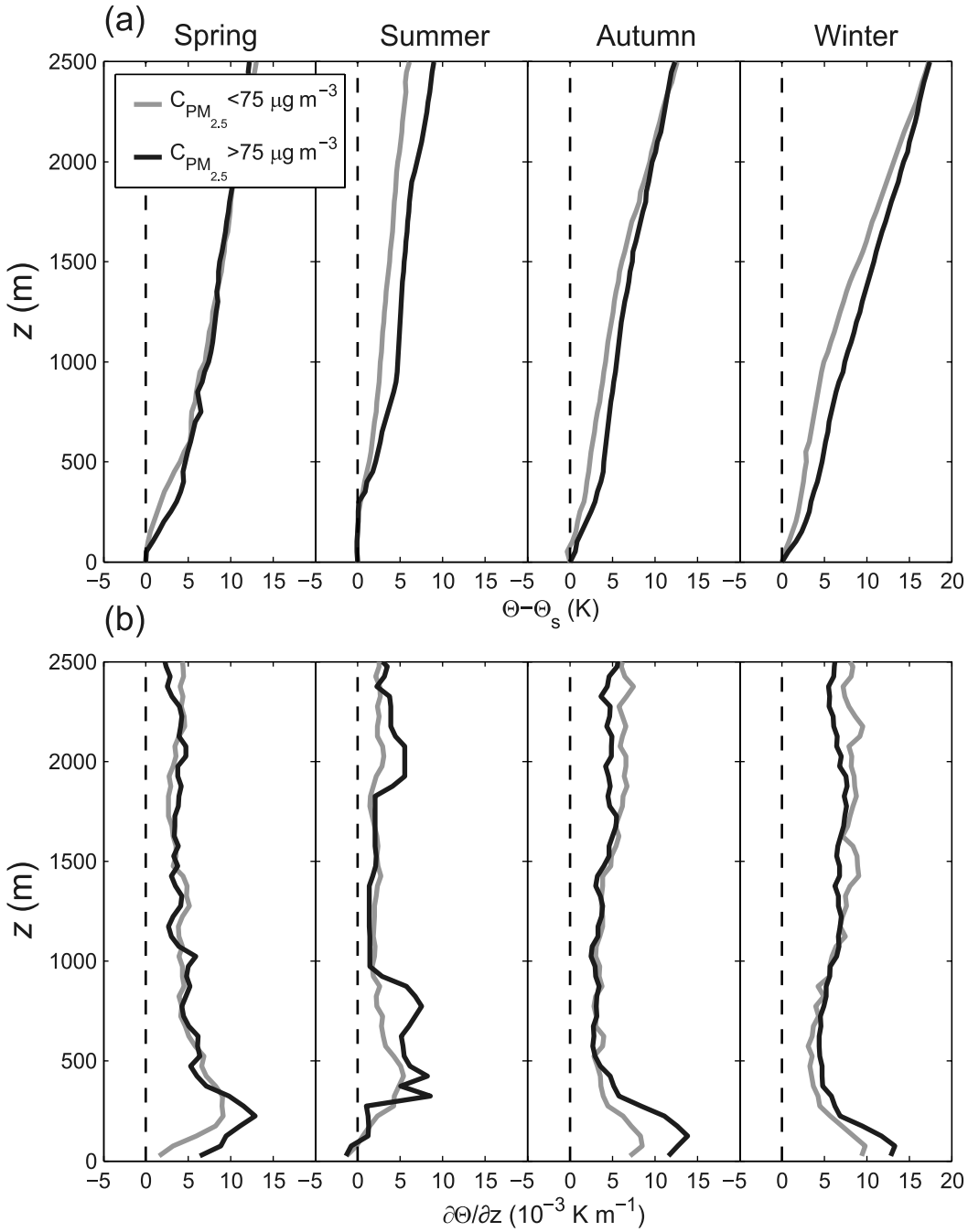

Fig. 4. Comparison of the mean profiles of (a) potential temperature (minus surface value Θ_s) and (b) potential temperature gradient, at 0800 LST on light air pollution days (mean nighttime $PM_{2.5}$ mass concentration lower than 75 μg m^{-3}) and heavy air pollution days (mean nighttime $PM_{2.5}$ mass concentration higher than 75 μg m^{-3}). The zero value lines are also shown.

PBLH is predicted by using the measured SHF and the retrieved SHF respectively, and the difference can be obtained. The linear fit of the data shown in Fig. 2c is given by

$$\frac{(Q_H - Q_{H_b})}{Q_{H_b}} = -0.0025\Delta CC_{PM_{2.5}} + 0.02 \,. \quad (8)$$

According to Eq. (8), Q_{H_b} is retrieved from the measurement data of Q_H. In this study, the retrieved Q_{H_b} is regarded as $Q_{H_{cln}}$. Although Eq. (8) is obtained from the data measured from 1000 LST to 1600 LST (the reason has been explained previously), this relationship is also applied to the data from 0800 LST to 1000 LST to obtain the retrieved SHF during this period, under the condition of no increment of aerosol loading, because the prediction of the PBLH begins at 0800 LST. The relative change in the retrieved $Q_{H_{cln}}$ is still treated as a function of $\Delta CC_{PM_{2.5}}$, and the data are plotted in Fig. 6 (for comparison purposes, the original data are also drawn in the figure). The linear fit of the data (red line) shows that $(Q_H - Q_{H_b})/Q_{H_b}$ does not vary with $\Delta CC_{PM_{2.5}}$, suggesting that the effect of aerosols on the SHF has been removed by

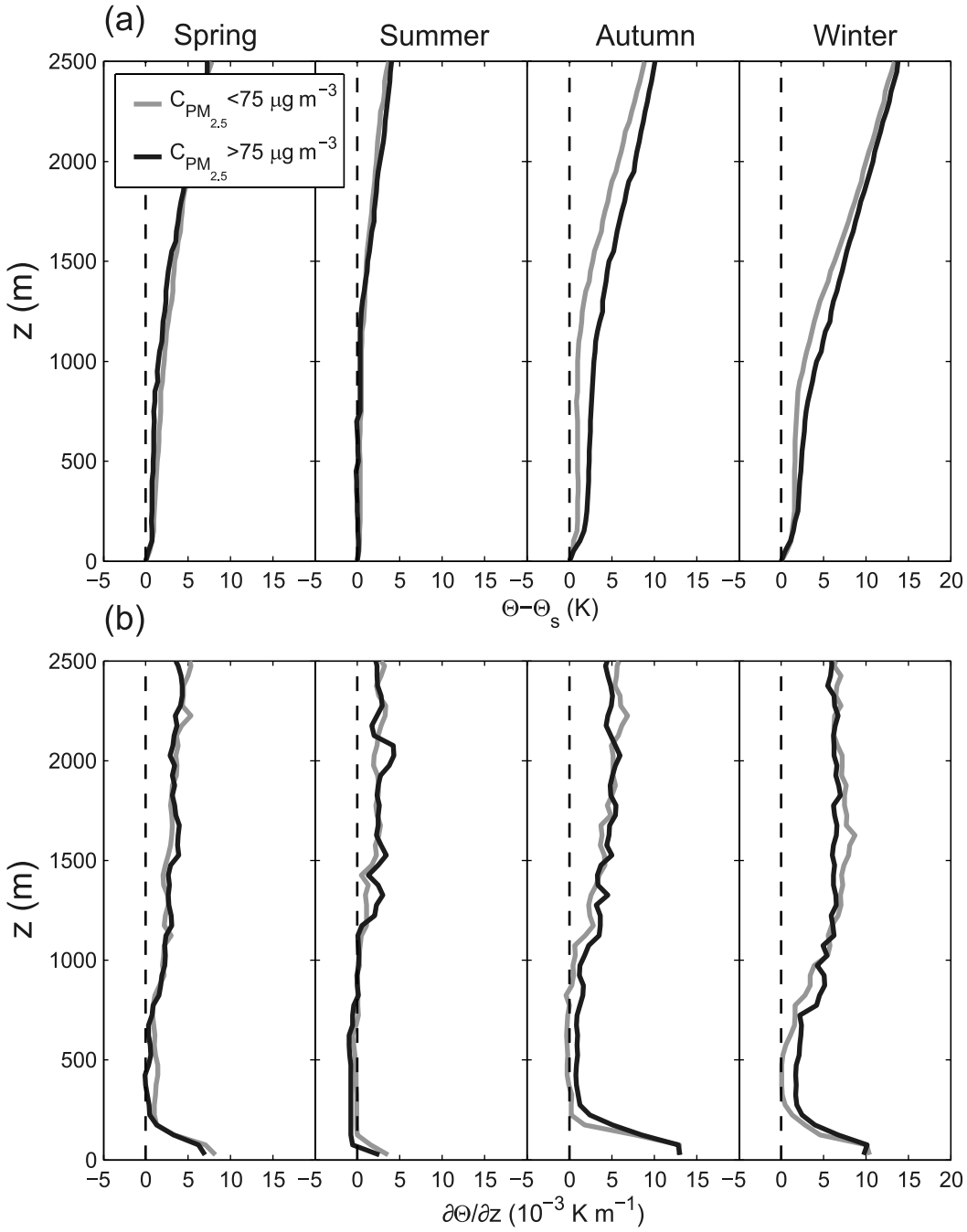

Fig. 5. As in Fig. 4 but at 2000 LST on light air pollution days (mean daytime $PM_{2.5}$ mass concentration lower than 75 μg m^{-3}) and heavy air pollution days (mean daytime $PM_{2.5}$ mass concentration higher than 75 μg m^{-3}). In summer, the mean daytime $PM_{2.5}$ mass concentration never exceeds 75 μg m^{-3} during the observation period.

the retrieval calculation. This means that the retrieved $Q_{H_{\rm cln}}$ can represent the SHF on the corresponding clean days, in which the real situation is that the aerosol loading is in excess of the background amount.

The PBLH at a certain time is the integrated result of continuous surface heating before this time. The accumulative effect of aerosols on CBL development should be considered to characterize the influence of aerosols in this period. Thus, we define the integration-averaged column mass concentration of $PM_{2.5}$, $ICC_{PM_{2.5}}$, to represent the aerosol loading from 0800 LST to the moment t. The expression reads

$$\mathrm{ICC}_{\mathrm{PM}_{2.5}} = \frac{1}{t-8}\int_{8}^{t} \mathrm{CC}_{\mathrm{PM}_{2.5}}\,\mathrm{d}t\,, \tag{9}$$

where t is time, starting at 0800 LST, and the unit is hours. We choose two moments to compare the difference in the

PBLH between the two situations with and without the increment of aerosol loading. By choosing t = 1200 LST, we compare the difference in the PBLH at noon. By choosing t = 1600 LST, we compare the difference in the PBLH at the moment (in the afternoon) when it usually reaches its maximum height during daytime.

According to Eq. (2), and by using the measured SHF and the profile of the potential temperature, the PBLH on polluted days is predicted and denoted as z_{i_R}. Also, by using the retrieved SHF and the same profile of the potential temperature, the PBLH on the clean days (which are assumed to have the same aerosol amount as the background days) is predicted and denoted as $z_{i_{CL}}$. Thus, the difference in the PBLH induced by the aerosol effect at a certain time is obtained, i.e., $\Delta z_i = z_{i_R} - z_{i_{CL}}$. At t = 1200 LST, the PBLH difference is denoted as $\Delta z_{i_{noon}}$. At t = 1600 LST, the PBLH difference is denoted as $\Delta z_{i_{day}}$. Its negative value means that the PBLH is reduced. Regarding $\Delta z_{i_{noon}}$ or $\Delta z_{i_{day}}$ as a function of $\mathrm{ICC}_{\mathrm{PM}_{2.5}}$, the data are plotted in Fig. 7. The fitting curves are expressed as:

$$\Delta z_{i_{noon}} = -0.010\mathrm{ICC}^2_{\mathrm{PM}_{2.5}} + 9.8; \quad (10a)$$

$$\Delta z_{i_{day}} = -0.012\mathrm{ICC}^2_{\mathrm{PM}_{2.5}} + 20.2. \quad (10b)$$

The data show that both $\Delta z_{i_{noon}}$ and $\Delta z_{i_{day}}$ increase with increasing $\mathrm{ICC}_{\mathrm{PM}_{2.5}}$, indicating that the larger amount of aerosol loading in the PBL results in the larger decrement of the PBLH. Also, the values of $\mathrm{ICC}_{\mathrm{PM}_{2.5}}$ at 1600 LST are larger than those at 1200 LST, suggesting that polluted air is accumulated in the afternoon and the amount of aerosol loading is increased. As shown in Fig. 1, the $\mathrm{PM}_{2.5}$ mass concentration at the surface is usually smaller during the daytime than at night. But, on some days, the $\mathrm{PM}_{2.5}$ mass concentration at surface increases without decreasing in the afternoon (e.g., 22–24, 26, 28, 29, and 31 December 2013). The rapid decrease in the $\mathrm{PM}_{2.5}$ mass concentration in the later afternoon on 26 December 2013 is caused by the blowing winds. The results shown in Fig. 7 indicate that the decrease in the PBLH at 1600 LST is significantly larger than at 1200 LST on the high polluted days. The maximum decrease in the PBLH at 1200 LST is about 200 m. The maximum decrease in the PBLH at 1600 LST is about 350–400 m. Our observation-based results are consistent with the numerical simulations reported in Wang et al. (2015), in which it was shown that a decrease in the PBLH at local noontime (0600 UTC) reaches 250–300 m during haze episodes over the Beijing–Tianjin–Hebei area, China, in July 2008. Figure 7 further shows that the relationship between $\Delta z_{i_{day}}$ (or $\Delta z_{i_{noon}}$) and $\mathrm{ICC}_{\mathrm{PM}_{2.5}}$ is not linear. The increasing rate of $\Delta z_{i_{day}}$ (as well as $\Delta z_{i_{noon}}$) increases with the magnitude of $\mathrm{ICC}_{\mathrm{PM}_{2.5}}$. According to the fitting curve for 1600 LST, i.e., Eq. (10b), when the daytime mean column mass concentration of $\mathrm{PM}_{2.5}$ reaches 200 mg m^{-2}, the decrease in the PBLH at 1600 LST is about 450 m. The nonlinear reduction of the PBLH related to aerosols means that, at a high level of aerosol loading, the same increase in aerosol amount results in a larger decrease in the PBLH. This reduction will lead to a higher $\mathrm{PM}_{2.5}$ mass concentration near the ground and an enhancement of air pollution levels at lower heights. This also suggests that urban areas have more opportunities to suffer from heavy air pollution, because the aerosol loading in such areas, especially in China, is maintained at a relatively high level.

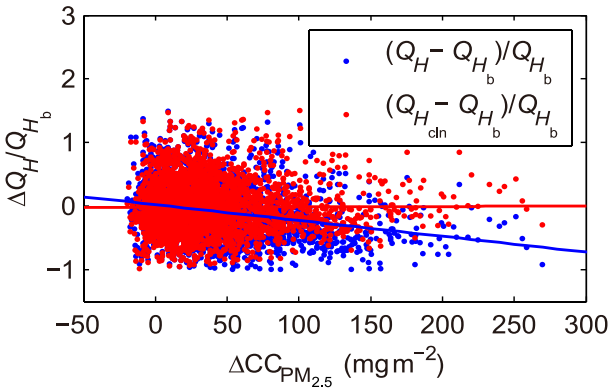

Fig. 6. Relative change in the retrieved SHF (red dots), as well as the original SHF (blue dots), as a function of the increment of the column mass concentration of $\mathrm{PM}_{2.5}$. The lines represent the linear fit of the data.

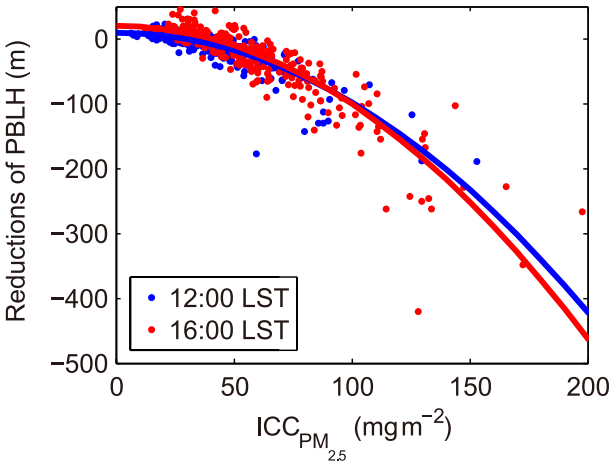

Fig. 7. Difference in PBLH between the air pollution days and clean days as a function of the vertically integration averaged column mass concentration of $\mathrm{PM}_{2.5}$ at 1200 LST (blue dots) and 1600 LST (red dots). The lines are the fitting curves.

4. Summary and discussion

This paper presents findings from two years of measurements of the DSR, DLR, SHF and $\mathrm{PM}_{2.5}$ mass concentration at the SORPES supersite in Nanjing, China. The data on clear-sky days show that the DSR and SHF decrease, while the DLR increases, with increasing aerosol loading. The statistics show that on the background days (i.e., the relatively low polluted days) the daytime mean $\mathrm{PM}_{2.5}$ mass concentration is of the order of 34.3 μg m^{-3}, while for all the

clear-sky days the daytime mean $PM_{2.5}$ mass concentration is about 72.7 μg m^{-3}. The increase in the aerosol loading to high levels leads to a daytime mean decrease in the DSR by 67.1 W m^{-2}, a decrease of the SHF by 9.6 W m^{-2}, and an increase in the DLR by 19.2 W m^{-2}. We also find that the daytime mean $PM_{2.5}$ mass concentration varies significantly with season. The seasonal mean of the $PM_{2.5}$ mass concentration during the daytime is about 103.9 μg m^{-3} in winter, 42.3 μg m^{-3} in summer, and 66.9 μg m^{-3} and 77.7 μg m^{-3} in spring and autumn, respectively. The seasonal mean reduction of the DSR during the daytime caused by aerosols is found to be the largest (about 82.1 W m^{-2}) in summer, the smallest (52.2 W m^{-2}) in spring, and about 71.5 W m^{-2} and 62.7 W m^{-2} in autumn and winter, respectively. The seasonal mean reduction in the SHF during the daytime is the largest (16.9 W m^{-2}) in autumn, the smallest (4.1 W m^{-2}) in summer, and about 10.6 W m^{-2} and 6.8 W m^{-2} in spring and winter, respectively. On the other hand, the seasonal mean increase in the DLR during the daytime caused by aerosols is the largest (about 29.6 W m^{-2}) in winter, the smallest (6.7 W m^{-2}) in summer, and about 20.3 W m^{-2} and 20.4 W m^{-2} in spring and autumn, respectively. These observational results provide useful information on the magnitude of aerosol direct radiative forcing in the Yangtze River Delta region, China.

Based on the statistical relationship between the SHF and aerosol loading [Eq. (8)], the SHF under clean-air conditions (i.e., only with background aerosols) can be derived from the observed SHF values. Using the SHF derived under clean-air conditions and the observed SHF values, together with the profile of the potential temperature (derived by radiosonde data), the evolution of the PBLH during the daytime under clean-air and normal conditions (i.e., with increased aerosols) can be predicted separately, and the decrease in the PBLH caused by aerosol loading can be estimated by the difference in the PBLH under clean-air conditions and normal conditions. Our results show that, at 1600 LST, when the PBL is usually at its highest level, the maximum decrease in the PBLH during the observation period reaches 350–400 m. Furthermore, the decreasing rate of the PBLH with aerosol loading increases more rapidly under high aerosol loading. Our results reveal how high aerosol levels can influence the PBLH, as well as explain why areas with high levels of aerosol loading often suffer from high levels of air pollution.

The radiosonde data show that high aerosol loading can significantly increase the atmospheric stability in the PBL during both daytime and nighttime. The potential temperature profile data at 2000 LST provide evidence that the solar irradiance reduction by aerosols during the daytime may hamper CBL development and reduce the PBLH by decreasing the entrainment process. The details of the CBL developing process under high air pollution conditions are not clear and should be investigated further. At 0800 LST, the atmosphere in the PBL on high polluted days is more stable than on low polluted days. This phenomenon mainly occurs in autumn and winter and means that, on heavy air pollution days, the CBL develops in a more stable background atmosphere. However, when we compare the difference in the PBLH between air pollution days and clean days, we still use the potential temperature profile at 0800 LST on the polluted days to predict the PBLH on the clean days. This treatment is expected to underestimate the PBLH on clean days and, consequently, the aerosol-induced PBLH reduction.

It should be pointed out that the aerosol-induced PBLH reduction in this study is based only on the reduction of the SHF values caused by aerosols. The heating effect of the absorbing aerosols on the atmospheric stability is not considered due to a lack of observations on the vertical distribution of aerosols. Yu et al. (2002) showed that aerosol absorption not only decreases SHFs within the PBL, but also increases the solar heating in the lower atmosphere. This heating effect decreases the strength of capping inversion and results in a rise in the PBLH, which compensates the decrease in the PBLH due to the reduced SHF. On the other hand, Barbaro et al. (2013) reported that the heating of absorbing aerosols in the atmosphere deepens the inversion layer and stabilizes the upper boundary layer, which further suppresses the development of the CBL in addition to the reduction of SHF. These effects should be included in future studies when more detailed observations become available, such as the vertical profiles of aerosols, by using, for example, the laser remote sensing (lidar) technique.

Acknowledgements. This work was supported by the National Natural Science Foundation of China (Grant No. 91544231), the State Key Research and Development Program of China (Grant No. 2016YFC0200500), and Jiangsu Provincial Collaborative Innovation Center of Climate Change. Jun ZOU was also supported by the Program for Outstanding PhD Candidates of Nanjing University. The authors thank the anonymous reviewers, whose comments helped greatly to improve the manuscript.

APPENDIX A

Comparison of $CC_{PM_{2.5}}$ and AOD

Here, we compare the estimated column concentration $CC_{PM_{2.5}}$ with the measured AOD at the wavelength of 500 nm. Figure A1 shows that a linear relationship exists between $CC_{PM_{2.5}}$ and AOD, although the data are somewhat scattered. For the uppermost data points in Fig. A1, the values of $CC_{PM_{2.5}}$ seem to be overestimated (the relative errors are larger than 50%). These data points correspond to the heavy air pollution days, on which turbulent mixing is suppressed, and the aerosols concentrate in the lower part of the PBL (Liu et al., 2009). In this situation, $CC_{PM_{2.5}}$ may be overestimated by Eq. (3). Another reason may be that the PBLH on the high polluted days is somewhat overestimated, as discussed in section 3.3, which can also result in overestimated $CC_{PM_{2.5}}$ values. Nevertheless, most data fall within the ±50% bias range, suggesting that the linear relationship is correct. Therefore, the derived $CC_{PM_{2.5}}$ can represent the column aerosol burden well.

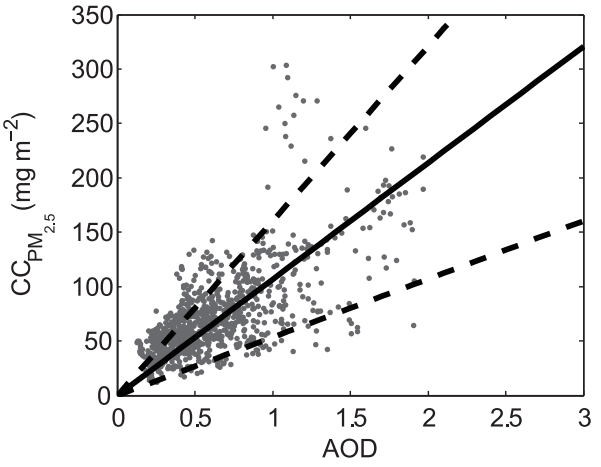

Fig. A1. Comparison of $CC_{PM_{2.5}}$ and AOD. The column concentration $CC_{PM_{2.5}}$ is estimated using Eq. (3). AOD is measured by a sunphotometer (CE-318) at the wavelength of 500 nm. The solid line represents the linear fitting relation, and the two dashed lines represent the bias range of ±50%.

REFERENCES

Barbaro, E., J. V.-G. de Arellano, M. C. Krol, and A. A. M. Holtslag, 2013: Impacts of aerosol shortwave radiation absorption on the dynamics of an idealized convective atmospheric boundary layer. *Bound.-Layer Meteor.*, **148**, 31–49, doi: 10.1007/s10546-013-9800-7.

Batchvarova, E., and S.-E. Gryning, 1991: Applied model for the growth of the daytime mixed layer. *Bound.-Layer Meteor.*, **56**, 261–274, doi: 10.1007/BF00120423.

Bush, B. C., and F. P. J. Valero, 2003: Surface aerosol radiative forcing at Gosan during the ACE-Asia campaign. *J. Geophys. Res.*, **108**(D23), 8660, doi: 10.1029/2002JD003233.

Chen, C. H., H. X. Wang, J. G. Huang, L. Zhang, G. Y. Qin, and J. M. Wang, 1994: Radiative effects of urban aerosols and their influence on mixed layer development. *Chinese Science Bulletin*, **39**, 56–61.

Deardorff, J. W., G. E. Willis, and B. H. Stockton, 1980: Laboratory studies of the entrainment zone of a convectively mixed layer. *J. Fluid. Mech.*, **100**, 41–64, doi: 10.1017/S0022112080001000.

Ding, A. J., T. Wang, V. Thouret, J.-P. Cammas, and P. Nédélec, 2008: Tropospheric ozone climatology over Beijing: Analysis of aircraft data from the MOZAIC program. *Atmos. Chem. Phys.*, **8**, 1–13, doi: 10.5194/acp-8-1-2008.

Ding, A. J., and Coauthors, 2013a: Intense atmospheric pollution modifies weather: A case of mixed biomass burning with fossil fuel combustion pollution in eastern China. *Atmos. Chem. Phys.*, **13**, 10 545–10 554, doi: 10.5194/acp-13-10545-2013.

Ding, A. J., and Coauthors, 2013b: Ozone and fine particle in the western Yangtze River Delta: An overview of 1 yr data at the SORPES station. *Atmos. Chem. Phys.*, **13**, 5813–5830, doi: 10.5194/acp-13-5813-2013.

Ding, A. J., and Coauthors, 2016: Enhanced haze pollution by black carbon in megacities in China. *Geophy. Res. Lett.*, **43**, 2873–2879, doi: 10.1002/2016GL067745.

Fedorovich, E., R. Conzemius, and D. Mironov, 2004: Convective entrainment into a shear-free, linearly stratified atmosphere: Bulk models reevaluated through large eddy simulations. *J. Atmos. Sci.*, **61**, 281–295, doi: 10.1175/1520-0469(2004)061<0281:CEIASL>2.0.CO;2.

Feng, J. L., M. Zhong, B. H. Xu, Y. Du, M. H. Wu, H. L. Wang, and C. H. Chen, 2014: Concentrations, seasonal and diurnal variations of black carbon in $PM_{2.5}$ in Shanghai, China. *Atmos. Res.*, **147–148**, 1–9, doi: 10.1016/j.atmosres.2014.04.018.

Gomes, L., M. Mallet, J. C. Roger, and P. Dubuisson, 2008: Effects of the physical and optical properties of urban aerosols measured during the CAPITOUL summer campaign on the local direct radiative forcing. *Meteor. Atmos. Phys.*, **102**, 289–306, doi: 10.1007/s00703-008-0321-8.

Huang, X., and Coauthors, 2016: Effects of aerosol–radiation interaction on precipitation during biomass-burning season in East China. *Atmos. Chem. Phys.*, **16**, 10 063–10 082, doi: 10.5194/acp-16-10063-2016.

Johnson, B. T., B. Heese, S. A. McFarlane, P. Chazette, A. Jones, and N. Bellouin, 2008: Vertical distribution and radiative effects of mineral dust and biomass burning aerosol over West Africa during DABEX. *J. Geophys. Res.*, **113**, D00C12, doi: 10.1029/2008JD009848.

Kaimal, J. C., and J. J. Finnigan, 1994: *Atmospheric Boundary Layer Flows: Their Structure and Measurement*. Oxford University Press, 289 pp.

Kaufman, Y. J., D. Tanré, and O. Boucher, 2002: A satellite view of aerosols in the climate system. *Nature*, **419**, 215–223, doi: 10.1038/nature01091.

Kessomkiat, W., H-J. H. Franssen, A. Graf, and H. Vereecken, 2013: Estimating random errors of eddy covariance data: An extended two-tower approach. *Agricultural and Forest Meteorology*, **171–172**, 203–219, doi: 10.1016/j.agrformet.2012.11.019.

Liao, H., W. Y. Chang, and Y. Yang, 2015: Climatic effects of air pollutants over china: A review. *Adv. Atmos. Sci.*, **32**(1), 115–139, doi: 10.1007/s00376-014-0013-x.

Liu, P. F., C. S. Zhao, Q. Zhang, Z. Z. Deng, M. Y. Huang, X. C. Ma, and X. X. Tie, 2009: Aircraft study of aerosol vertical distributions over Beijing and their optical properties. *Tellus B*, **61**, 756–767, http://dx.doi.org/10.1111/j.1600-0889.2009.00440.x.

Mukund, V., D. K. Singh, V. K. Ponnulakshmi, G. Subramanian, and K. R. Sreenivas, 2014: Field and laboratory experiments on aerosol-induced cooling in the nocturnal boundary layer. *Quart. J. Roy. Meteor. Soc.*, **140**, 151–169, doi: 10.1002/qj.2113.

Nordbo, A., L. Järvi, S. Haapanala, J. Moilanen, and T. Vesala, 2013: Intra-city variation in urban morphology and turbulence structure in Helsinki, Finland. *Bound.-Layer Meteor.*, **146**, 469–496, doi: 10.1007/s10546-012-9773-y.

Offerle, B., C. S. B. Grimmond, and T. R. Oke, 2003: Parameterization of net all-wave radiation for urban areas. *J. Appl. Meteor.*, **42**, 1157–1173, doi: 10.1175/1520-0450(2003)042<1157:PONARF>2.0.CO;2.

Satheesh, S. K., and K. K. Moorthy, 2005: Radiative effects of natural aerosols: A review. *Atmos. Environ.*, **39**, 2089–2110, doi: 10.1016/j.atmosenv.2004.12.029.

Schotanus, P., F. T. M. Nieuwstadt, and H. A. R. de Bruin, 1983: Temperature measurement with a sonic anemometer and its application to heat and moisture fluxes. *Bound.-Layer Meteor.*, **26**, 81–93, doi: 10.1007/BF00164332.

Stull, R. B., 1976: The energetics of entrainment across a density interface. *J. Atmos. Sci.*, **33**, 1260–1267, doi: 10.1175/1520-

0469(1976)033<1260:TEOEAD>2.0.CO;2.

Stull, R. B., 1988: *An Introduction to Boundary Layer Meteorology*. Springer, 670 pp.

Sühring, M., B. Maronga, F. Herbort, and S. Raasch, 2014: On the effect of surface heat-flux heterogeneities on the mixed-layer-top entrainment. *Bound.-Layer Meteor.*, **151**, 531–556, doi: 10.1007/s10546-014-9913-7.

Sun, J. N., 2009: On the parameterization of convective entrainment: Inherent relationships among entrainment parameters in bulk models. *Adv. Atmos. Sci.*, **26**(5), 1005–1014, doi: 10.1007/s00376-009-7222-8.

van Zanten, M. C., P. G. Duynkerke, and J. W. M. Cuijpers, 1999: Entrainment parameterization in convective boundary layers. *J. Atmos. Sci.*, **56**, 813–828, doi: 10.1175/1520-0469(1999)056<0813:EPICBL>2.0.CO;2.

Wang, H., and Coauthors, 2015: Mesoscale modeling study of the interactions between aerosols and PBL meteorology during a haze episode in Jing–Jin–Ji (China) and its nearby surrounding region–Part 1: Aerosol distributions and meteorological features. *Atmos. Chem. Phys.*, **15**, 3257–3275, doi: 10.5194/acp-15-3257-2015.

Wong, D. C., and Coauthors, 2012: WRF-CMAQ two-way coupled system with aerosol feedback: Software development and preliminary results. *Geoscientific Model Development*, **5**, 299–312, doi: 10.5194/gmd-5-299-2012.

Yu, H., and Coauthors, 2006: A review of measurement-based assessments of the aerosol direct radiative effect and forcing. *Atmos. Chem. Phys.*, **6**, 613–666, doi: 10.5194/acp-6-613-2006.

Yu, H. B., S. C. Liu, and R. E. Dickinson, 2002: Radiative effects of aerosols on the evolution of the atmospheric boundary layer. *J. Geophys. Res.*, **107**(D12), doi: 10.1029/2001JD000754.

Zhao, S. Y., and Coauthors, 2015: Seasonal variation and four-year trend of black carbon in the Mid-west China: The analysis of the ambient measurement and WRF-Chem modeling. *Atmos. Environ.*, **123**, 430–439, doi: 10.1016/j.atmosenv.2015.05.008.

Zhuang, B. L., and Coauthors, 2017: The surface aerosol optical properties in the urban area of Nanjing, west Yangtze River Delta, China. *Atmos. Chem. Phys.*, **17**, 1143–1160, doi: 10.5194/acp-17-1143-2017.